Research article

FGL2 improves experimental colitis related to gut microbiota structure and bile acid metabolism by regulating macrophage autophagy and apoptosis

Yuan Zhao [a], Zheng Xiang [a], Haoran Pan [a], Xielin Huang [b], Weizhen Chen [a], Zhiming Huang [a,*]

[a] *Department of Gastroenterology and Hepatology, The First Affiliated Hospital of Wenzhou Medical University, Wenzhou, 325000, China*
[b] *Department of Gastrointestinal Surgery, The First Affiliated Hospital of Wenzhou Medical University, Wenzhou, 325000, China*

A R T I C L E   I N F O

A B S T R A C T

Inflammatory bowel disease (IBD) is a refractory disease with immune abnormalities and pathological changes. Intestinal macrophages are considered to be the main factor in establishing and maintaining intestinal homeostasis. The immunoregulatory and anti-inflammatory activity of fibrinogen-like protein 2 (FGL2) can regulate macrophage polarization. However, its function in IBD is unclear. In this study, we explored the effect of FGL2 on macrophage polarization, autophagy, and apoptosis in bone marrow-derived macrophages (BMDMs) treated with lipopolysaccharide (LPS) and further investigated changes in the intestinal barrier, flora, and bile acid in dextran sodium sulfate (DSS)-treated mice. Our results demonstrated that $FGL2^{-/-}$ weakened ERK signaling to promote M1 polarization and upregulate inflammation, autophagy, and apoptosis in LPS-stimulated BMDMs. rFGL2 treatment reversed these effects. $FGL2^{-/-}$ mice exhibited higher sensitivity to DSS exposure, with faster body weight loss, shorter colon lengths, and higher disease activity index (DAI) values. rFGL2 treatment protected against experimental ulcerative colitis (UC), restrained excessive autophagy, apoptosis, and improved gut barrier impairment. Gut microbiota structure and bile acid homeostasis were more unbalanced in $FGL2^{-/-}$ DSS mice than in wild-type (WT) DSS mice. rFGL2 treatment improved gut microbiota structure and bile acid homeostasis. Altogether, our results established that FGL2 is a potential therapeutic target for IBD.

1. Introduction

Inflammatory bowel disease (IBD), including Crohn's disease (CD) and ulcerative colitis (UC), is a group of idiopathic inflammation-related bowel diseases with clinical symptoms including abdominal pain, rectal bleeding, weight loss, diarrhea, and

anemia requiring life-long medication [1,2]. Recent investigations found that the morbidity of IBD has increased worldwide. However, the etiology and pathogenesis are complex and remain poorly understood [3,4]. Disturbances in intestinal microbiota homeostasis, as well as environmental, genetic, and infectious factors, may serve as vital factors to trigger intestinal immune system abnormalities and inflammatory reactions, finally resulting in IBD [5–8]. Some studies indicated that patients with IBD are more susceptible to developing colorectal cancer [9,10], but few therapeutic drugs are available to alleviate or treat IBD. Thus, preventing IBD at an early stage or developing a new type of drug to treat IBD is extremely necessary and important.

The gastrointestinal tract is the largest chamber of the immune system, in which intestinal macrophages are considered to play key roles in establishing and maintaining intestinal homeostasis and preventing excessive immune responses [11]. Normally, macrophages are divided into M1 and M2 phenotypes, with the M1 phenotype displaying pro-inflammatory characteristics and the M2 phenotype exhibiting anti-inflammatory and immunosuppressive features [12]. However, abnormal immune responses and excessive inflammation can damage the gut itself and the intestinal mucosal barrier, leading to certain intestinal diseases such as IBD [12,13]. Therefore, regulating abnormal inflammation and immune responses mediated by intestinal macrophages may be a potential and promising strategy for treating IBD.

Previous studies revealed that the gut microbiota regulates the host immune system and serves as an immune modulator through its metabolites, such as bile acids, or by releasing other factors [14,15]. Clinically, researchers have observed changes in the microbiota composition and bile acids in IBD [16,17]. Specifically, both *Firmicutes* and *Bacteroidetes* were reduced, whereas *Proteobacteria* was increased in IBD patients [18]. Duboc et al. [17] observed that gut microbiota imbalance led to modifications in the luminal bile acids (BA) pool composition, and altered BA composition in the gut lumen eliminated the anti-inflammatory effects of some BA species on intestinal epithelial cells and may be involved in the chronic inflammation of IBD. Several studies demonstrated that commensal or probiotic bacteria, such as *Bifidobacterium* and *Escherichia coli* Nissle, attenuated the chronic inflammation of dextran sulfate sodium (DSS) colitis [19–21]. Fecal transplantation from colitis mice to wild-type (WT) mice resulted in colitis inflammation [22]. Therefore, maintaining intestinal microbiota homeostasis may be an effective method to relieve the chronic inflammation of IBD.

FGL2 is a member of the fibrinogen-associated protein family, which is divided into the membrane-bound type (mfgl2) with coagulation activity and the secretory type (sfgl2) with immunosuppressive characteristics [23]. Several studies indicated that FGL2 was upregulated in fulminant hepatitis, spontaneous abortion, xenograft rejection, ischemia-reperfusion injury, sepsis, and other inflammatory models and played a great role in the initiation and progression of these inflammatory diseases [24–27]. Previously, our clinical study reported that FGL2 was upregulated in patients with active IBD [28]. FGL2 levels were significantly positively related to disease activity index values, the erythrocyte sedimentation rate and C-reactive protein levels in patients [29]. However, the role of the protein in IBD is not clear.

This study assessed the effect of FGL2 on macrophages in a DSS-induced colitis mouse model to probe the effect of FGL2 on the development of IBD and changes in intestinal microbiota and BA.

2. Materials and methods

2.1. Animals

FGL2$^{-/-}$ mice on a C57BL/6 background mice were by Nanjing Biomedical Research Institute of Nanjing University (Nanjing, China). We make FGL2 knockout mice via CRISPR/Cas9 system. Cas9 mRNA, sgRNA will be co-injected into zygotes. sgRNA direct Cas9 endonuclease cleavage of FGL2 gene and create a DSB (double-strand break). Such breaks will be repaired by non-homologous end joining (NHEJ). So FGL2 gene will be disrupted by frameshift mutation from exon1. Finally, we obtained FGL2$^{-/-}$mice, which carry the 128-bp deletion mutation. Germline transmission was confirmed by RT-PCR.

Thirty male mice (6–8 weeks, 22–27 g in weight) in this study were randomly divided into five groups, with six mice in each group. The mice were reared in a specific pathogen-free environment (12 h light/dark cycles and 24 ± 2 °C). In this study, we follow the animal experiments ethical code, which is to replace, reduce, and refine. The experimental animals operating procedures were ratified by the Experimental Animal Management Committee of Wenzhou Medical University_ (WYDW20170074).

2.2. Induction of colitis and treatment

Inducing colitis with DSS (MP Biomedicals, USA) is a commonly used IBD model [30]. Briefly, 2.5 % DSS was orally administered for 8 days in sterile water. The WT mice and FGL2$^{-/-}$ mice drank sterile water. In consideration of the plasma half-life of recombinant FGL2 (rFGL2), 20 μg of rFGL2 (R&D Systems, USA) was given to FGL2$^{-/-}$ mice by tail vein injection on days 0, 1, 3, 5, and 7 [31]. The mice were monitored daily during the experiment, including weight loss, diarrhea, and hematochezia. Disease activity index (DAI) values were used to evaluate the extent of intestinal injury [32]. These parameters were graded according to a previously defined standard scoring system: body weight loss: 0 (no loss), 1 (1%–5%), 2 (5%–10 %), 3 (10%–20 %), and 4 (>20 %); stool bleeding: 0 (no blood), 1 (hemoccult-positive), 2 (hemoccult-positive and gross blood in the stool), and 4 (gross bleeding); stool consistency: 0 (normal), 2 (loose stool), and 4 (diarrhea). All mice were euthanized under anesthesia on day 8 after collecting eyeball blood, liver, and colon samples.

2.3. Cell culture and sample treatment

Bone marrow-derived macrophages (BMDM) were obtained from WT mice and FGL2$^{-/-}$ mice through the tibia and fibula [33]. In

brief, bone marrow was flushed from the femurs and tibias, cultured, and differentiated in bone marrow growth medium comprised of Dulbecco's modified Eagle medium (Gibco, USA) supplemented with 10 % fetal bovine serum (Gibco, USA), 20 ng/mL macrophage colony-stimulating factor (PeproTech, China), and 1 % penicillin/streptomycin (Gibco, USA) at 37 °C in a humidified incubator with 5 % CO_2. The bone marrow cell growth medium was changed every 2 days. After 7 days of cultivation, we obtained M0 macrophages, which were used in the subsequent experiments. Some groups were stimulated with 100 ng/mL lipopolysaccharide (LPS) (PeproTech, China) for 24 h, while others were incubated with 5 μg/mL rFGL2 for 24 h and then stimulated with 100 ng/mL LPS for 24 h.

2.4. Cytokine analysis by enzyme-linked immunosorbent assay

Interleukin (IL)-6, IL-1β, and tumor necrosis factor (TNF)-α in blood and in colon tissue samples were determined using an enzyme-linked immunosorbent assay (ELISA) kit (MultiScience, China) as described in the manufacturer's instructions.

2.5. Western blotting

Proteins were extracted from cells, colonic, and hepatic samples. Protein concentrations were calculated using a bicinchoninic acid kit. Proteins were separated by sodium dodecyl sulfate-polyacrylamide gel electrophoresis and transferred to polyvinylidene membranes. After blocking with 5 % (w/v) skimmed milk, the membranes were incubated overnight with the following primary antibodies: FGL2 (1:500, ProteinTech, China), iNOS (1:1000, Affinity, China), Cox-2 (1:1000, ProteinTech, China), LC3B (1:2000, Abcam, USA), p62 (1:1000, HuaBio, China), Bcl-2 (1:1000, Affinity, China), C-caspase3 (1:1000, ProteinTech, China), cytochrome C (1:1000, HuaBio, China), CYP7A1 (1:500, Affinity, China), ZO-1 (1:500, Servicebio, China), occuldin (1:500, Servicebio, China), ERK (1:1000, Abmart, China), *p*-ERK (1:1000, Abmart, China), and GAPDH (1:10000, Abcam, USA). The next day, the membranes were incubated with secondary antibodies for 2 h at room temperature. The membranes were visualized using an enhanced chemiluminescence system. Image Laboratory 3.0 software (Bio-Rad, USA) was used to quantify the band intensity.

2.6. Quantitative real-time polymerase chain reaction

Total RNA was isolated from ileum tissues using TRIZOL reagent and then reverse-transcribed using PrimerScript reverse transcriptase (TaKaRa, Japan). The primer sequences were: mouse FXR 5′-GGCAGAATCTGGATTTGGAATCG-3′ (forward) and 5′-GCCCAGGTTGGAATAGTAAGACG-3′ (reverse); mouse FGF15 5′-ATGGCGAGAAAGTGGAACGG-3′ (forward) and 5′-GGACCAGCG-GAGTACAGGT-3′ (reverse); mouse GAPDH (5′-AGGTCGGTGTGAACGGATTTG-3′ (forward) and 5′-TGTAGACCATGTAGTTGAGGTCA-3′ (reverse). GAPDH was used as the endogenous reference, and polymerase chain reaction (PCR) results were analyzed by the ΔΔCt-method.

2.7. Hematoxylin and eosin staining

Mouse colon and hepatic tissue specimens were fixed in 4 % paraformaldehyde and embedded in paraffin. Then, each specimen was cut into 4 μm thick tissue sections and stained with hematoxylin and eosin (H&E). The microstructure of the tissues was estimated by optical microscopy (Nikon, Japan). Histological analysis was graded according to a previously defined scoring system [34].

2.8. Immunohistochemical analysis

The above-treated samples were deparaffinized with xylene and rehydrated through a graded ethanol bath. Afterward, the sections were washed and blocked with 3 % (v/v) hydrogen peroxide. Then, the sections were kept in 10.2 mM sodium citrate buffer at 95 °C for 20 min and blocked with 10 % (w/v) bovine serum albumin phosphate-buffered saline for 10 min. Finally, the sections were incubated overnight in primary antibodies at 4 °C. Then, the sections were incubated with horseradish peroxidase-conjugated secondary antibody and counterstained with hematoxylin. The images were obtained using a fluorescence microscope at 200 × magnification.
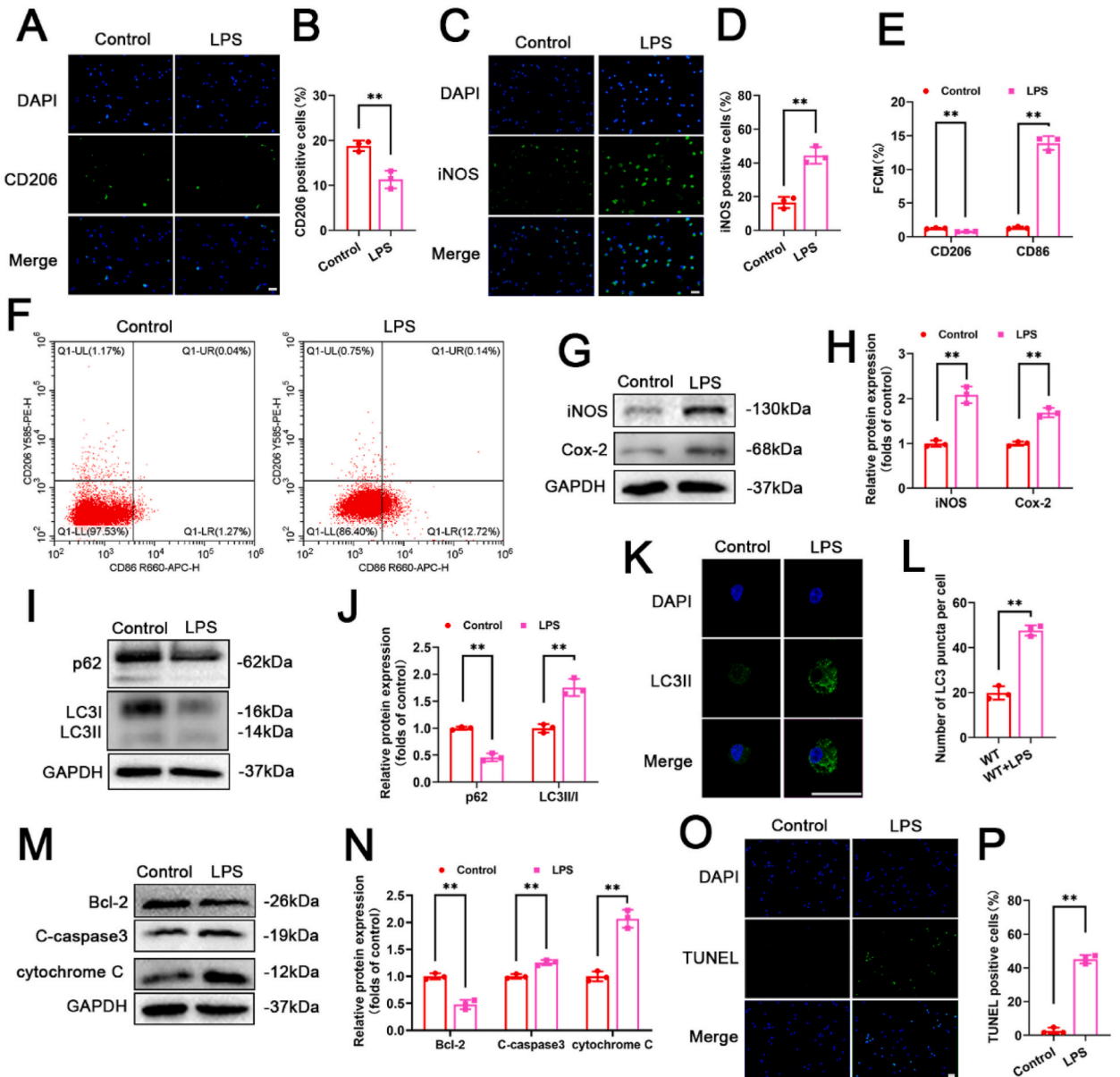
2.9. Immunofluorescence staining

Cells were fixed in 4 % paraformaldehyde for 15 min, then permeabilized with 0.3 % Triton X-100 for 10 min at room temperature, incubated with 10 % (w/v) bovine serum albumin phosphate-buffered saline for 1 h at 37 °C, and incubated with primary antibodies against inducible nitric oxide synthase (iNOS) (1:100, Affinity, China), CD206 (1:100, Affinity, China), and LC3B (1:200, Abcam, USA) overnight at 4 °C. Subsequently, the cells were incubated with the secondary antibody at 37 °C for 1h and the nuclei were stained with 4′,6-diamidino-2-phenylindole (DAPI) for 10 min. Staining was analyzed by fluorescence microscopy.

2.10. TUNEL staining

Cells were fixed in 4 % paraformaldehyde for 15 min, then permeabilized with 0.3 % Triton X-100 for 10 min at room temperature. Next, the cells were stained with a TdT-mediated dUTP nick end labeling (TUNEL) Kit (Yeasen Biotechnology, China) at 37 °C for 1h, and the nuclei were stained with DAPI for 10 min. Staining was analyzed by fluorescence microscopy.

2.11. Flow cytometric analysis

BMDMs were collected and stained with PE-*anti*-CD206 (Biolegend, China), APC-*anti*-CD86 (Multisciences, China), or specific isotype antibodies (eBioscience, USA). The cells were analyzed using a FACS Calibur flow cytometer, and the data were processed with

Fig. 1. LPS reduces M2 polarization and promotes M1 polarization, autophagy, and apoptosis in the BMDMs **(A, C)** CD206 and iNOS positive cells in 2 groups were evaluated by immunofluorescence (original magnification × 200, scale bar: 50 μm). **(B, D)** Statistical chart of the number of CD206 and iNOS positive cells in 2 groups. **(E)** Statistical chart of CD206 and CD86. **(F)** Flow cytometry of CD206 and CD86 in 2 groups. **(G)** Western blotting of iNOS and Cox-2 in the Control and LPS groups. All the gel electrophoresis experiments were carried out under the same experimental conditions. **(H)** Statistical chart of the quantification of iNOS and Cox-2. **(I)** Western blotting of p62 and LC3II/I in the Control and LPS groups. All the gel electrophoresis experiments were carried out under the same experimental conditions. **(J)** Statistical chart of the quantification of p62 and LC3II/I. **(K)** LC3II-positive autophagic vesicles were detected by immunofluorescence (original magnification × 400; scale bar: 100 μm). **(L)** Statistical chart of LC3II-positive autophagic vesicles. **(M)** Western blotting of Bcl-2, cytochrome C, and C-caspase 3 in the Control and LPS groups. All the gel electrophoresis experiments were carried out under the same experimental conditions. **(N)** Statistical chart of the quantification of Bcl-2, cytochrome C, and C-caspase 3. **(O)** TUNEL assay in 2 groups were evaluated by immunofluorescence (original magnification × 200, scale bar: 50 μm). **(P)** Statistical chart of the quantification of apoptotic positive cells. The obtained data were expressed as means ± SD and representative of three independent experiments. $**P < 0.01$, $*P < 0.05$.
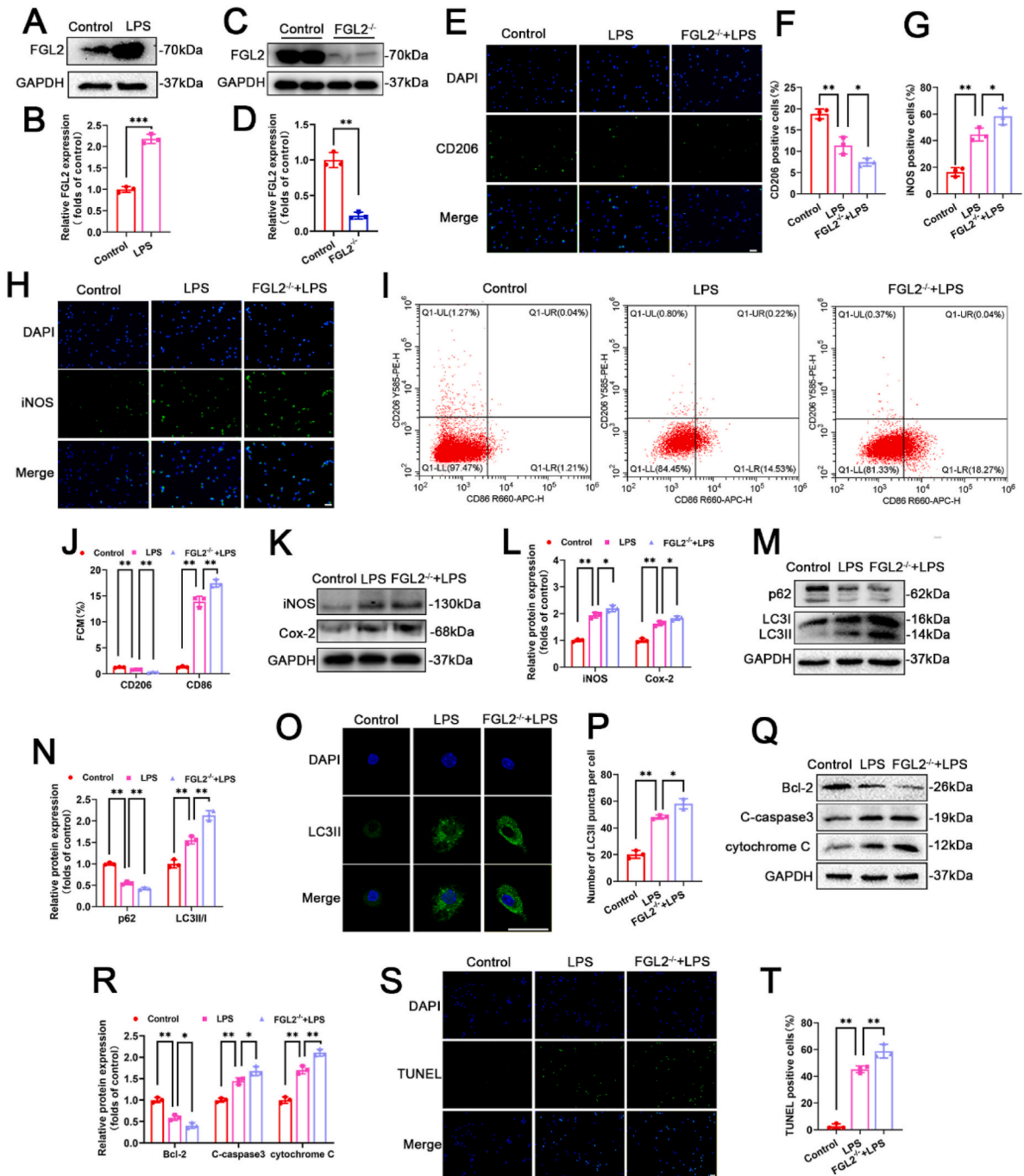
Fig. 2. FGL2 deficiency downregulates M2 polarization and upregulates M1 polarization, autophagy, and apoptosis in LPS-stimulated BMDMs (A) Western blotting of FGL2 in 2 groups. All the gel electrophoresis experiments were carried out under the same experimental conditions. **(B)** Statistical chart of the quantification of FGL2. **(C)** Western blotting of FGL2 knockout rate in the FGL2$^{-/-}$ group. All the gel electrophoresis experiments were carried out under the same experimental conditions. **(D)** Statistical chart of the quantification of FGL2 knockout rate. **(E, H)** CD206 and iNOS positive cells in each group were evaluated by immunofluorescence (original magnification × 200, scale bar: 50 μm). **(F, G)** Statistical chart of the number of CD206 and iNOS positive cells in each group. **(I)** Flow cytometry of CD206 and CD86 in the Control, LPS, and FGL2$^{-/-}$ + LPS groups. **(J)** Statistical chart of CD206 and CD86. **(K)** Western blotting of iNOS and Cox-2 in the Control, LPS, and FGL2$^{-/-}$ + LPS groups. All the gel electrophoresis experiments were carried out under the same experimental conditions. **(L)** Statistical chart of the quantification of iNOS and Cox-2. **(M)** Western blotting of p62 and LC3II/I in the Control, LPS, and FGL2$^{-/-}$ + LPS groups. All the gel electrophoresis experiments were carried out under the same experimental conditions. **(N)** Statistical chart of the quantification of p62 and LC3II/I. **(O)** LC3II-positive autophagic vesicles were detected by immunofluorescence (original magnification × 400; scale bar: 100 μm). **(P)** Statistical chart of LC3II-positive autophagic vesicles. **(Q)** Western blotting of Bcl-2, cytochrome C and C-caspase 3 in the Control, LPS and FGL2$^{-/-}$ + LPS groups. All the gel electrophoresis experiments were carried

out under the same experimental conditions. **(R)** Statistical chart of the quantification of Bcl-2, cytochrome C and C-caspase 3. **(S)** TUNEL assay in each group were evaluated by immunofluorescence (original magnification × 200, scale bar: 50 μm). **(T)** Statistical chart of the quantification of apoptotic positive cells. The obtained data were expressed as means ± SD and representative of three independent experiments. **$P < 0.01$, *$P < 0.05$.

CytExpert software.

2.12. 16S rRNA sequencing and analysis

A total of 30 fecal samples were collected from the 2 control groups and mice treated with DSS for 8 days and then stored at −80 °C. Nucleic acid was extracted using a fecal genomic DNA extraction kit (Tiangen Biotech (Beijing)), and the concentration was measured. The variable V3–V4 region of 16S rRNA was amplified using the primers 338F (5′- ACTCCTACGGGAGGCAGCA-3′) and 806R (5′-GGACTACHVGGGTWTCTAAT-3′), then the product was purified and recovered. Computer sequencing was performed on the constructed library using Illumina novaseq6000 (novaseq6000, Illumina) to obtain raw data (BMKcloud, Beijing, China). QIIME2 software was utilized to analyze alpha diversity, principal coordinates analysis, the species distribution histogram, heatmap, linear discriminant analysis effect size, and functional prediction.

2.13. Biochemical analysis

Serum total bile acid (TBA) levels were determined using an automatic biochemical analyzer (Rayto, China).

2.14. Statistical analysis

GraphPad Prism version 7.00 (GraphPad Software, Inc, USA) was used for all statistical analyses. The data are expressed as the mean ± standard deviation (SD). The independent-sample *t*-test and one-way ANOVA were used as appropriate. P-values of <0.05 were considered statistically significant.

3. Results

3.1. LPS reduces M2 polarization and promotes M1 polarization, autophagy, and apoptosis in the BMDMs

LPS treatment was used to simulate the inflammatory reaction of IBD in BMDMs *in vitro*. Compared to the control group, the LPS group showed a higher number of iNOS-positive cells and a lower number of CD206-positive cells (Fig. 1A–D). We next tested for the presence of BMDM subpopulations using flow cytometry. The expression of CD206 was lower, and the expression of CD86 was higher in the LPS group compared to the control group (Fig. 1E and F). The Western blotting results indicated that the levels of iNOS and Cox-2 in the LPS group were significantly higher than those in the control group (Fig. 1G and H). Nest, we quantified LC3II (autophagosomal protein) and SQSTM1/p62 (autophagic substrate protein) protein expression. The Western blotting results exhibited a lower level of p62 but a higher level of LC3II in the LPS group than the control group (Fig. 1I and J). The immunofluorescence assay showed that the number of LC3II puncta per cell in the LPS group was higher than that of the control group (Fig. 1K and L). The level of apoptosis in BMDMs was also changed. Western blotting analysis showed a lower level of Bcl-2 but higher levels of C-caspase3 and cytochrome C in the LPS group than in the control group (Fig. 1M and N). The TUNEL staining results showed a higher number of TUNEL-positive cells in the LPS group than in the control group (Fig. 1O and P). These results indicate that LPS downregulated M2 polarization and upregulated M1 polarization, autophagy, and apoptosis in the BMDMs.

3.2. FGL2 deficiency downregulates M2 polarization and upregulates M1 polarization, autophagy, and apoptosis in LPS-stimulated BMDMs

The expression of FGL2 was increased in the LPS-stimulated BMDMs *in vitro* (Fig. 2A and B). We knocked out FGL2 and verified the knockout efficiency of FGL2 to investigate the role of FGL2 in BMDMs (Fig. 2C and D). Under LPS stimulation, the number of CD206-positive cells decreased, and FGL2 knockout further decreased the number of CD206-positive cells (Fig. 2E and F). LPS stimulation increased the number of iNOS-positive cells, and FGL2 knockout further increased the iNOS-positive cells (Fig. 2G and H). Flow cytometry showed that under LPS stimulation, CD206 expression decreased and CD86 expression increased, while FGL2 deficiency further downregulated CD206 and upregulated CD86 (Fig. 2I and J). The Western blotting results showed that LPS stimulation increased iNOS and Cox-2 levels, and FGL2 knockout further increased these protein levels (Fig. 2K and L). Given the importance of macrophages in autophagy and apoptosis, we investigated whether FGL2 modulated autophagy and apoptosis. Western blotting analysis revealed decreases in p62 and increases in LC3II levels in the $FGL2^{-/-}$ + LPS group compared to the LPS group (Fig. 2M and N). The immunofluorescence assay further revealed that FGL2 knockout increased the number of LC3II puncta per cell (Fig. 2O and P). We also found that the apoptosis level in BMDMs was changed. Western blotting analysis showed a lower level of Bcl-2 but higher levels of C-caspase3 and cytochrome C in the $FGL2^{-/-}$ + LPS group than in the LPS group (Fig. 2Q and R). Additionally, FGL2 knockout increased the number of TUNEL-positive cells (Fig. 2S and T). These data suggest that FGL2 knockout increased the M1 phenotype and upregulated autophagy, as well as apoptosis, in BMDMs under LPS stimulation.
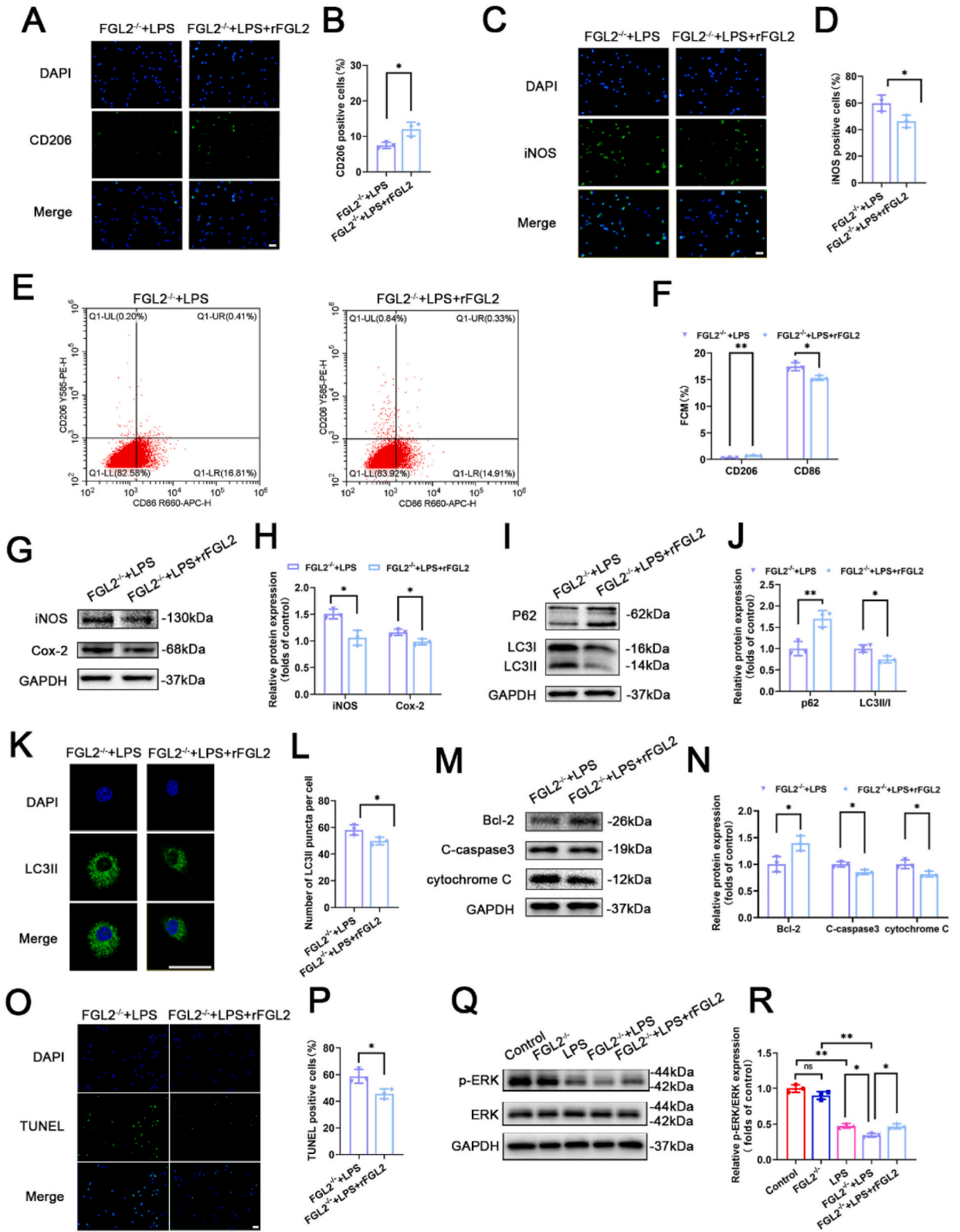
(caption on next page)

Fig. 3. FGL2 enhances ERK signaling to upregulate M2 polarization and downregulate M1 polarization, autophagy, and apoptosis in LPS-stimulated BMDMs **(A, C)** CD206 and iNOS positive cells in 2 group were evaluated by immunofluorescence (original magnification × 200, scale bar: 50 μm). **(B, D)** Statistical chart of the number of CD206 and iNOS positive cells in 2 group. **(E)** Flow cytometry of CD206 and CD86 in the FGL2$^{-/-}$ + LPS and FGL2$^{-/-}$ + LPS + rFGL2 groups. **(F)** Statistical chart of CD206 and CD86. **(G)** Western blotting of iNOS and Cox-2 in the FGL2$^{-/-}$ + LPS and FGL2$^{-/-}$ + LPS + rFGL2 groups. All the gel electrophoresis experiments were carried out under the same experimental conditions. **(H)** Statistical chart of the quantification of iNOS and Cox-2. **(I)** Western blotting of p62 and LC3II/I in the FGL2$^{-/-}$ + LPS and FGL2$^{-/-}$ + LPS + rFGL2 groups. All the gel electrophoresis experiments were carried out under the same experimental conditions. **(J)** Statistical chart of the quantification of p62 and LC3II/I. **(K)** LC3II-positive autophagic vesicles were detected by immunofluorescence (original magnification × 400; scale bar: 100 μm). **(L)** Statistical chart of LC3II-positive autophagic vesicles. **(M)** Western blotting of Bcl-2, cytochrome C and C-caspase 3 in the FGL2$^{-/-}$ + LPS and FGL2$^{-/-}$ + LPS + rFGL2 groups. All the gel electrophoresis experiments were carried out under the same experimental conditions. **(N)** Statistical chart of the quantification of Bcl-2, cytochrome C and C-caspase 3. **(O)** TUNEL assay in each group were evaluated by immunofluorescence (original magnification × 200, scale bar: 50 μm). **(P)** Statistical chart of the quantification of apoptotic positive cells. **(Q)** Western blotting of *p*-ERK and ERK in the LPS, FGL2$^{-/-}$ + LPS, and FGL2$^{-/-}$ + LPS + rFGL2 groups. All the gel electrophoresis experiments were carried out under the same experimental conditions. **(R)** Statistical chart of the quantification of *p*-ERK/ERK. The obtained data were expressed as means ± SD and representative of three independent experiments. *******P* < 0.01, ******P* < 0.05. rFGL2, recombinant FGL2.

3.3. FGL2 enhances ERK signaling to upregulate M2 polarization and downregulate M1 polarization, autophagy, and apoptosis in LPS-stimulated BMDMs

FGL2$^{-/-}$ BMDMs were treated with rFGL2 before LPS stimulation to further determine the function of FGL2 in macrophage polarization, autophagy, and apoptosis. The number of CD206-positive cells in the FGL2$^{-/-}$ + LPS + rFGL2 group was increased compared to the FGL2$^{-/-}$ + LPS group (Fig. 3A and B). Additionally, the number of iNOS-positive cells in the FGL2$^{-/-}$ + LPS + rFGL2 group was lower than in the FGL2$^{-/-}$ + LPS group (Fig. 3C and D). Flow cytometry showed a higher expression of CD206 but a lower expression of CD86 in the FGL2$^{-/-}$ + LPS + rFGL2 group compared to the FGL2$^{-/-}$ + LPS group (Fig. 3E and F). The Western blotting results revealed decreases in iNOS and Cox-2 levels in the FGL2$^{-/-}$ + LPS + rFGL2 group compared to the FGL2$^{-/-}$ + LPS group (Fig. 3G and H). We also found a higher level of p62 but a lower level of LC3II in the FGL2$^{-/-}$ + LPS + rFGL2 group compared to the FGL2$^{-/-}$ + LPS group (Fig. 3I and J). The immunofluorescence assay showed that the number of LC3II puncta per cell in the FGL2$^{-/-}$ + LPS + rFGL2 group was lower than that in the FGL2$^{-/-}$ + LPS group (Fig. 3K and L). Western blotting analysis showed a higher level of Bcl-2 but lower levels of C-caspase3 and cytochrome C in the FGL2$^{-/-}$ + LPS + rFGL2 group than in the FGL2$^{-/-}$ + LPS group (Fig. 3M and N). Consistently, TUNEL-positive cells were conspicuously decreased in the FGL2$^{-/-}$ + LPS + rFGL2 group compared to the FGL2$^{-/-}$ + LPS group (Fig. 3O and P). Previous studies reported that ERK played an essential role in regulating macrophage polarization and autophagy. Our results showed that the phosphorylation levels of ERK were decreased in the LPS and FGL2$^{-/-}$ + LPS groups compared to the control and FGL2$^{-/-}$ groups, respectively, and were further decreased after FGL2 knockout. However, rFGL2 treatment reversed the effect of FGL2 knockout (Fig. 3Q and R). To sum up, FGL2 may enhance ERK phosphorylation to regulate macrophage polarization and inhibit autophagy and apoptosis in BMDMs under LPS stimulation.
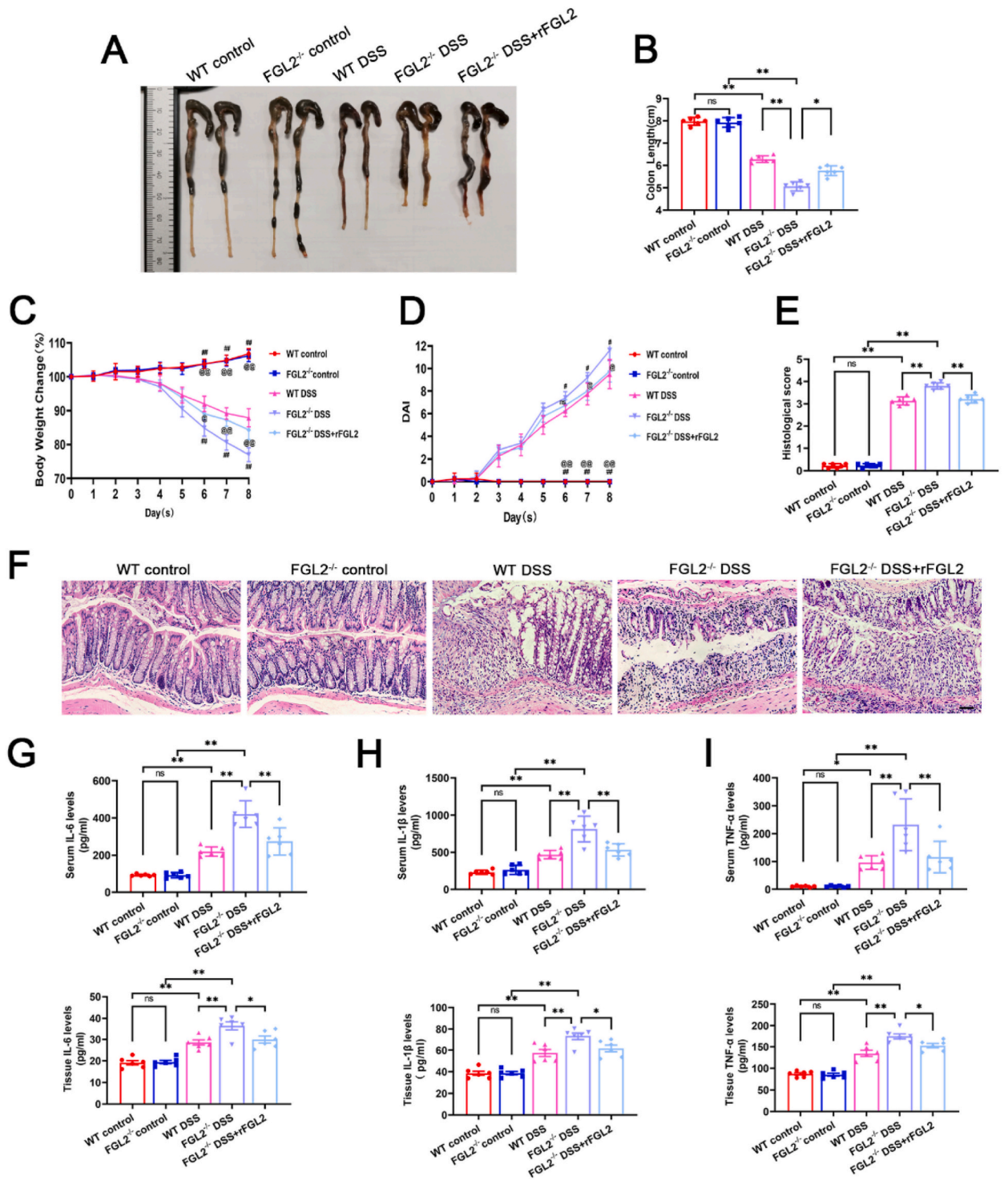
3.4. FGL2 deficiency sensitizes mice to experimental UC lesions with prominent inflammatory responses

We established an experimental colitis lesion model in WT and FGL2$^{-/-}$ mice using 2.5 % DSS to explore the role of FGL2 in maintaining intestinal homeostasis. As shown in Fig. 4A–D, all DSS-treated mice showed weight loss, increased disease activity, and shortened colon lengths compared with WT control and FGL2$^{-/-}$ control mice, respectively, indicating the successful generation of DSS-induced colitis. The FGL2$^{-/-}$ mice displayed higher sensitivity to DSS, including faster weight loss (Fig. 4C), higher DAI values (Fig. 4D), and shorter colon lengths compared to WT mice (Fig. 4A and B). However, rFGL2 treatment rescued those changes. Additionally, the histopathological alterations in the FGL2$^{-/-}$ mice after DSS treatment were more significant than those in the treated WT and rFGL2 mice, with increased epithelial cell destruction and inflammatory cell accumulation (Fig. 4E and F). An inflammatory reaction is one of the pathological characteristics of IBD, and we tested the inflammatory levels in each group of mice. Interestingly, the FGL2$^{-/-}$ DSS mice exhibited an overall increased inflammatory response, including elevated pro-inflammatory cytokine (TNF-α, IL-1β, and IL-6) concentrations in serum and tissue (Fig. 4G–I). These data provide evidence that FGL2 relieved inflammatory responses and protected colon tissue in the DSS-treated mice.

3.5. FGL2 protects against experimental UC by regulating macrophage polarization, autophagy, and apoptosis and maintaining the gut barrier

We analyzed changes in autophagy, apoptosis, and the gut barrier in different UC mice to further study the significance of FGL2 in IBD. As shown in Fig. 5A and B, immunohistochemical (IHC) analysis revealed that CD206 levels in the FGL2$^{-/-}$ DSS group were lower compared to the WT DSS group and rFGL2 treatment rescued CD206 downregulation. iNOS levels in the WT DSS and FGL2$^{-/-}$ DSS groups were higher compared to the WT control and FGL2$^{-/-}$ control groups, respectively, and FGL2 knockout further upregulated iNOS levels in DSS-treated mice. However, rFGL2 treatment reversed iNOS upregulation. The Western blotting results indicated increases in iNOS and Cox-2 levels in WT DSS and FGL2$^{-/-}$ DSS mice compared with WT control and FGL2$^{-/-}$ control mice, respectively (Fig. 5C and D). FGL2 knockout further increased iNOS and Cox-2 levels. However, rFGL2 treatment reversed the effects of FGL2 knockout (Fig. 5C and D). The FGL2$^{-/-}$ DSS group showed the lowest p62 level but the highest LC3II level among the WT control,

Fig. 4. FGL2 deficiency sensitizes mice to experimental UC lesions with prominent inflammatory responses **(A, B)** Macroscopic colon appearances and the lengths of colons from each group. **(C)** Body weight changes were calculated as the percent relative to original body weights. **(D)** DAI. **(E)** Statistical chart of the quantification of histological score. **(F)** H&E staining for colon tissues in each group (original magnification × 200, scale bar: 50 μm). **(G–I)** Statistical chart of the quantification of cytokines IL-6, IL-1β and TNF-α in each group. The obtained data were expressed as means ± SD and representative of three independent experiments, n = 6 per group. **$P < 0.01$, *$P < 0.05$. Compared with WT DSS, ##$P < 0.01$ and #$P < 0.05$; Compared with FGL2$^{-/-}$ DSS, @@$P < 0.01$ and @$P < 0.05$. ns, no significance. DAI, Disease activity index. H&E staining, Hematoxylin and eosin staining.
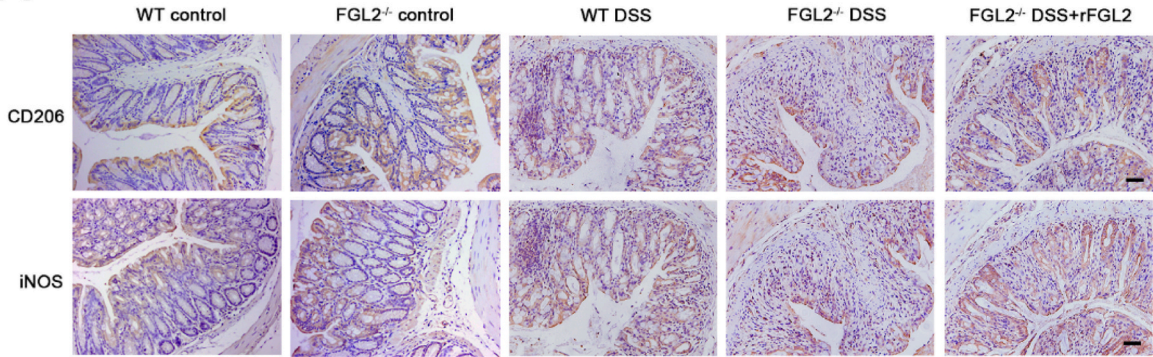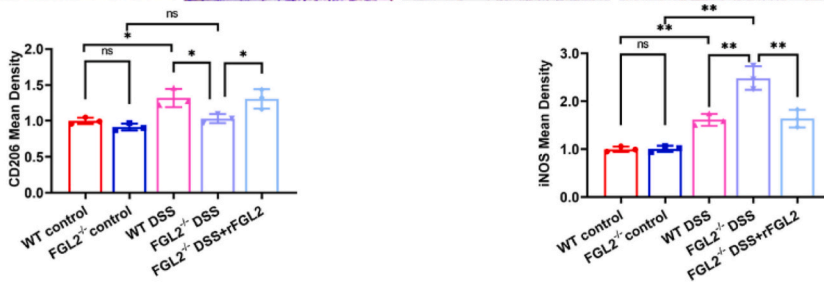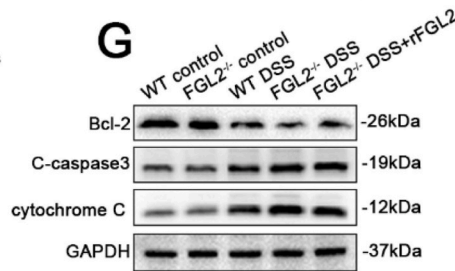
(caption on next page)
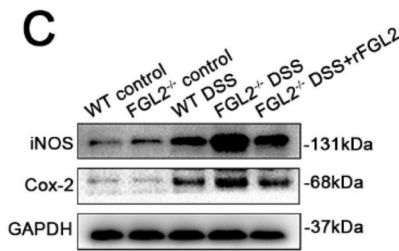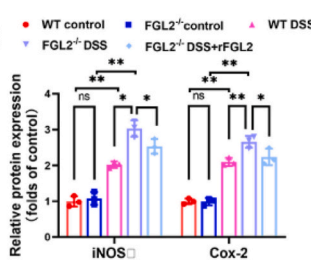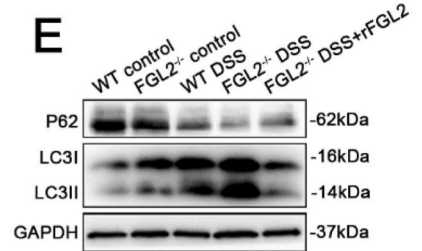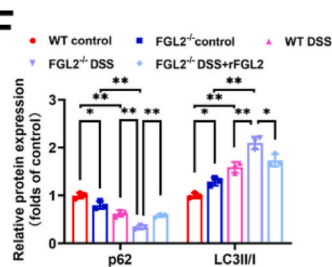
Fig. 5. FGL2 protects against experimental UC by regulating macrophage polarization, autophagy, and apoptosis and maintaining the gut barrier **(A)** IHC for CD206 and iNOS of colon tissues in each group (original magnification × 200, scale bar: 50 μm). **(B)** The statistical chart describes the CD206 and iNOS mean density. **(C)** Western blotting of iNOS and Cox-2 in each group. All the gel electrophoresis experiments were carried out under the same experimental conditions. **(D)** Statistical chart of the quantification of iNOS and Cox-2. **(E)** Western blotting of p62 and LC3II/I in each group. All the gel electrophoresis experiments were carried out under the same experimental conditions. **(F)** Statistical chart of the quantification of p62 and LC3II/I. **(G)** Western blotting o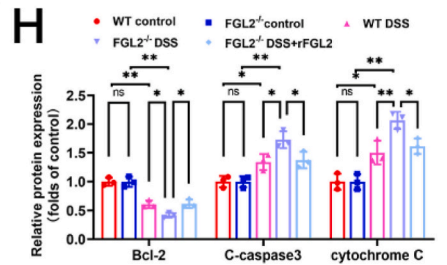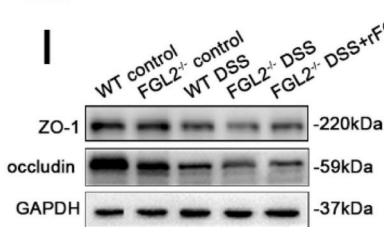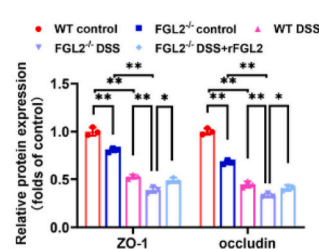f Bcl-2, cytochrome C and C-caspase 3 in each group. All the gel electrophoresis experiments were carried out under the same experimental conditions. **(H)** Statistical chart of the quantification of Bcl-2, cytochrome C and C-caspase 3. **(I)** Western blotting of ZO-1 and occludin in each group. All the gel electrophoresis experiments were carried out under the same experimental conditions. **(J)** Statistical chart of the quantification of ZO-1 and occludin. The obtained data were expressed as means ± SD and representative of three independent experiments, n = 6 per group. **$P < 0.01$, *$P < 0.05$. IHC, immunohistochemistry.

FGL2$^{-/-}$ control, WT DSS, and FGL2$^{-/-}$ DSS groups, and rFGL2 treatment reversed p62 and LC3II protein levels (Fig. 5E and F). In addition, both the WT DSS and FGL2$^{-/-}$ DSS groups showed lower Bcl-2 levels but higher level of C-caspase3 and cytochrome C levels compared to the WT control and FGL2$^{-/-}$ control groups, respectively, and FGL2 knockout exacerbated these changes (Fig. 5G and H). After treatment with rFGL2, Bcl-2 was significantly upregulated and C-caspase3, and cytochrome C were downregulated compared to the FGL2$^{-/-}$ DSS group (Fig. 5G and H). Finally, we found that intestinal barrier proteins ZO-1 and occludin were downregulated in the FGL2$^{-/-}$ control group and further downregulated in mice treated with DSS (Fig. 5I and J). FGL2 knockout exacerbated ZO-1 and occludin downregulation while rFGL2 treatment rescued these changes (Fig. 5I and J). These data demonstrated that FGL2 restrained excessive autophagy and apoptosis and protected the intestinal barrier in DSS-treated mice.

3.6. FGL2 improves gut microbiota structure in DSS-treated mice

Given that the gut microbiota changes in IBD patients, we examined the relationship between FGL2 and the gut microbiota in fecal samples by 16S rRNA gene sequencing. DSS treatment reduced the Chao index (Fig. 6A) and Shannon index (Fig. 6B) values to varying degrees compared with the 2 control groups, especially in the FGL2$^{-/-}$ DSS group, indicating that FGL2 deficiency could reduce alpha diversity, which reflects community diversity in experimental UC through species richness and evenness. Unifrac-based principal co-ordinates analysis (PCoA) (Fig. 6C) indicated distinct clusterings of microbial composition in the 5 groups.

At the phylum level, DSS model mice displayed a decrease in *Firmicutes* and *Bacteroidota* compared to the 2 control groups, whereas *Proteobacteria* was increased. FGL2 knockout exacerbated these changes. However, rFGL2 treatment reversed abnormal gut microbiota composition (Fig. 6D). At the genus level, 63 bacterial genera with differences among the 5 groups were selected by ANOVA, and the top 30 abundant genera were further used to identify the specific bacterial phylotypes altered by FGL2 (Fig. 6E and F). Twenty genera in the DSS group were significantly altered compared with the control group, while 36 genera underwent FGL2 deletion, and rFGL2 treatment altered 19 genera and exhibited a shift toward a healthier profile. The heatmap analysis showed that the absence of FGL2 further altered the gut microbiota composition in model mice, and rFGL2 treatment substantially reshaped the gut microbiota composition.

The bacterial genera with higher relative abundance (unclassified_*Lachnospiraceae* > unclassified_*Muribaculance* > *Lachnospiraceae*_NK4A136_group > *Escherichia/Shigella*) were all significantly different in FGL2$^{-/-}$ DSS mice compared with WT DSS and FGL2$^{-/}$$^{-}$ DSS + rFGL2 mice (Fig. 6G). Notably, FGL2 deficiency significantly enriched *Escherichia/Shigella* (0.006 % abundance in the WT control, 0.014 % in the FGL2$^{-/-}$ control, 0.505 % in WT DSS, 32.817 % in FGL2$^{-/-}$ DSS, and 1.750 % in FGL2$^{-/-}$ DSS + rFGL2), which was greatly reduced by rFGL2 treatment. Linear discriminant analysis effect size (LEfse) indicated that there were 3, 2, 3, 5, and 4 significant differences in the WT control, FGL2$^{-/-}$ control, WT DSS, FGL2$^{-/-}$ DSS, and FGL2$^{-/-}$ DSS + rFGL2 groups, respectively. These changes were manifested as an increased abundance of *Lachnospiraceae*_NK4A136_group, *Bacteroides, Blautia* and ASF356 (linear discriminate analysis (LDA) > 4.0) in the rFGL2-treated group, and increased *Mucispirillum, Akkermansia,* and *Romboutsia* in the FGL2$^{-/-}$ DSS group (Fig. 6H)

Next, we predicted the microbial community function using the Kyoto Encyclopedia of Genes and Genomes database (Fig. 6I). The pathways enriched in the microbiome of the WT DSS mice were "caprolactam degradation," "carotenoid biosynthesis," "metabolism of xenobiotics by cytochrome P450," and "drug metabolism-cytochrome P450." After FGL2-deficient mice were treated with DSS, the pathways enriched in the microbiome changed to the following: "tetracycline biosynthesis," "propanoate metabolism," "tryptophan metabolism," and "lysine degradation." However, in the rFGL2-treated group, the pathways enriched in the microbiome changed to "alanine, aspartate, and glutamate metabolism," "beta-lactam resistance," "biosynthesis of amino acids," "cyanoamino acid metabolism," and "phenylpropanoid biosynthesis." The above results showed that FGL2 improved the composition and structure of the intestinal microbiota in DSS-induced colitis mice.

3.7. FGL2 improves BA metabolism in DSS-treated mice

We analyzed the relevant indicators of BA to verify the effect of FGL2 on bile acid in UC mice. DSS-treated mice exhibited histological changes in liver tissue. H&E staining showed that the hepatocytes were swollen, and the hepatic sinusoids were narrowed in the model groups, especially in the FGL2$^{-/-}$ DSS group. However, rFGL2 treatment reversed these changes in liver tissue (Fig. 7A). Next, we measured serum TBA levels. TBA levels in the FGL2$^{-/-}$ DSS group were highest among the WT control, FGL2$^{-/-}$ control, and WT DSS groups, and rFGL2 treatment decreased TBA levels (Fig. 7B). Considering that the ileum is the main site for BA reabsorption, we investigated the mRNA expression level of FXR and FGF15 in the ileum of mice. As showed in Fig. 7C& and D, both the FXR and
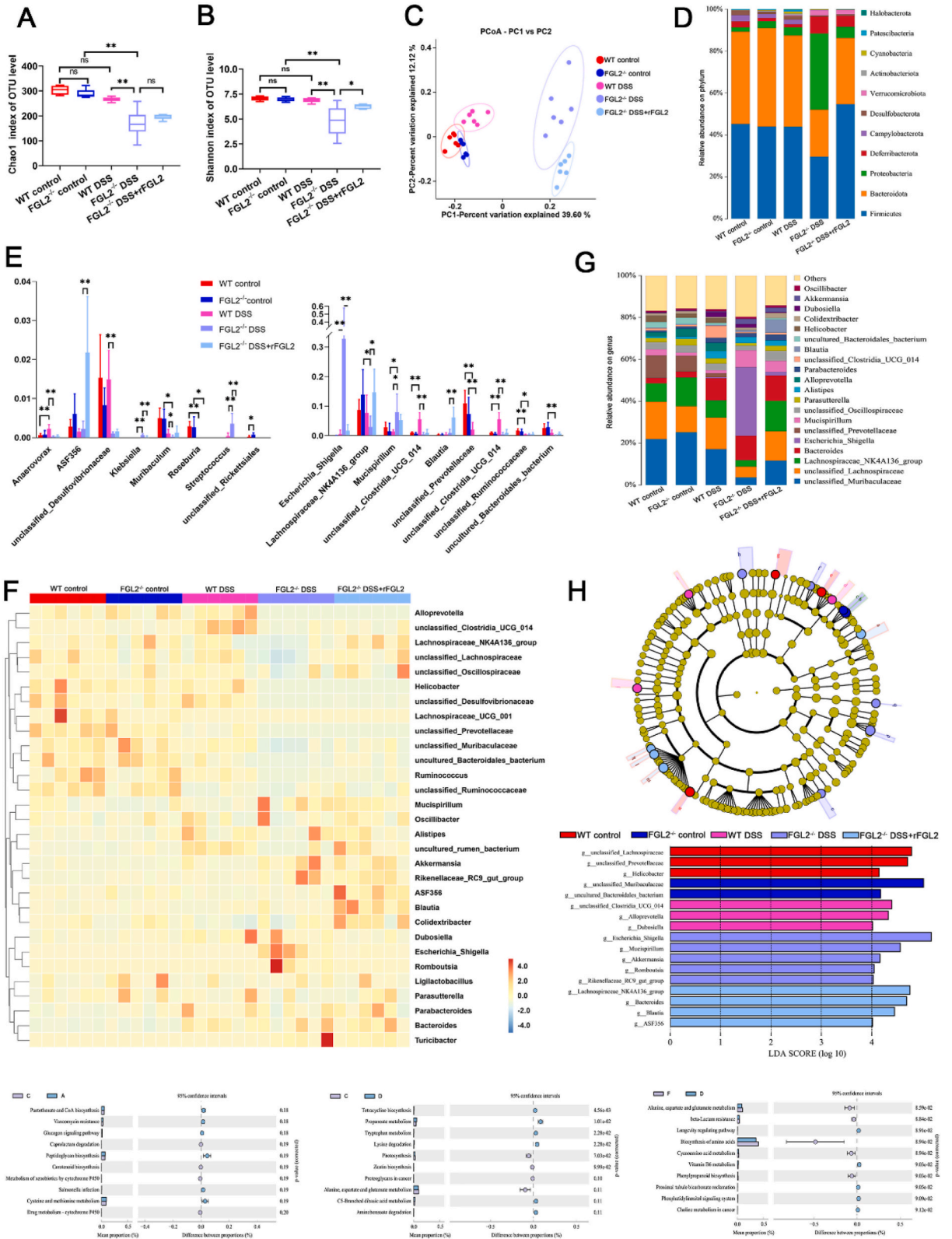
Fig. 6. FGL2 improves gut microbiota structure in DSS-treated mice **(A, B)** Gut microbiota α diversity analysis. **(C)** Unweighted Unifrac PCoA analysis. **(D)** Relative abundances of gut microbiota at the phylum level. **(E)** ANOVA analysis of differential bacteria at the genus level. **(F).** Relative abundances of top 30 genera in the heatmap. **(G)** Relative abundances of gut microbiota at the genus level. **(H)** Discriminative taxa were determined by LEfSe (log10 LDA >4.0). **(I)** Prediction of microbiome function based on KEGG database. n = 6 per group. **$P < 0.01$, *$P < 0.05$.
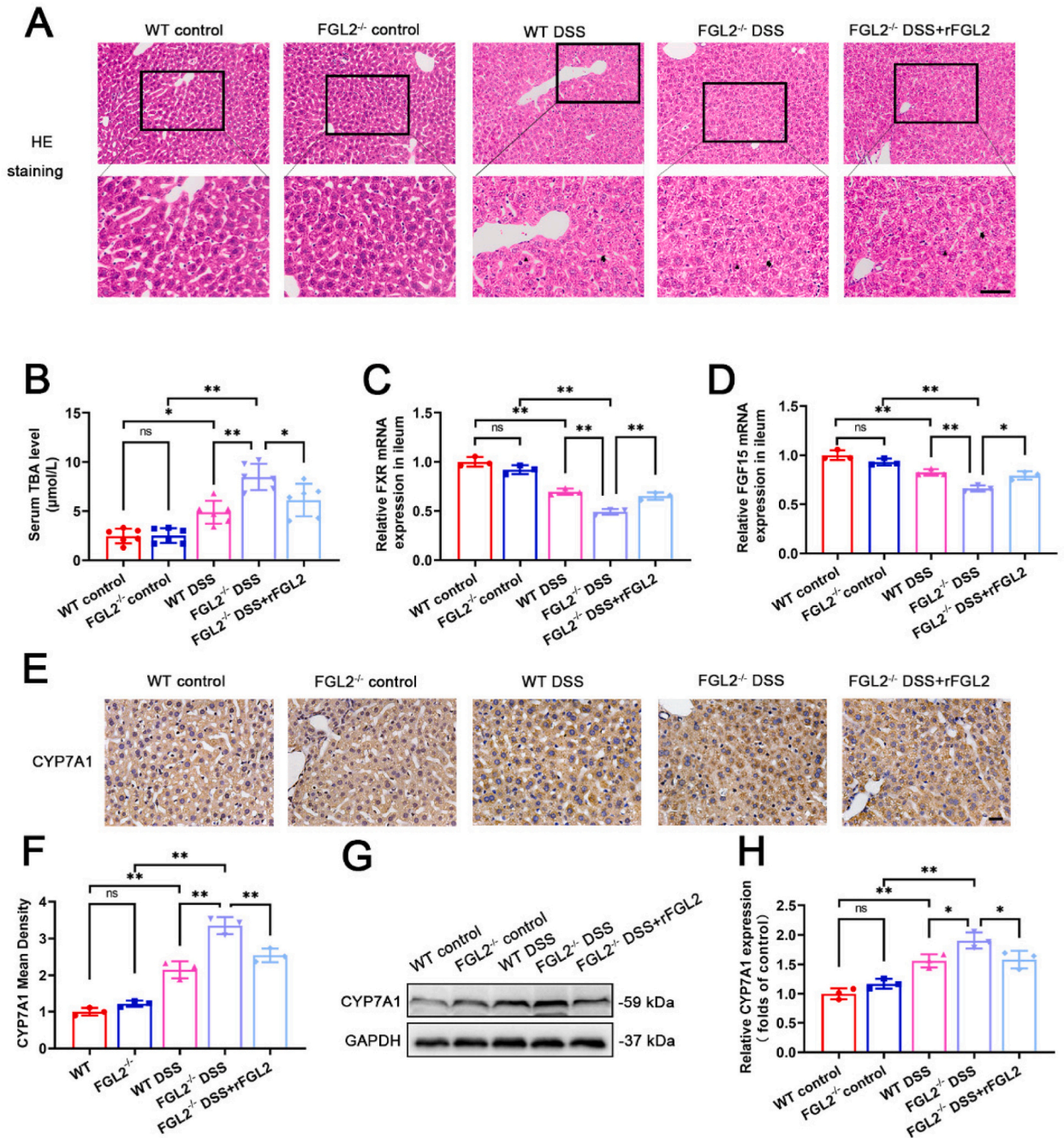
Fig. 7. FGL2 improves BA metabolism in DSS-treated mice **(A)** H&E staining for liver tissues in each group (original magnification × 200, scale bar: 50 μm). **(B)** Statistical chart of the quantification of TBA. **(C, D)** Statistical chart of the quantification of FXR mRNA and FGF15 mRNA. **(E)** IHC for CYP7A1 of liver tissues in each group (original magnification × 200, scale bar: 50 μm). **(F)** The statistical chart describes the CYP7A1 mean density. **(G)** Western blotting of CYP7A1 in each group. All the gel electrophoresis experiments were carried out under the same experimental conditions. **(H)** Statistical chart of the quantification of CYP7A1. The obtained data were expressed as means ± SD and representative of three independent experiments, n = 6 per group. **$P < 0.01$, *$P < 0.05$. IHC, immunohistochemistry. TBA, total bile acid.

FGF15 levels in the FGL2$^{-/-}$ DSS group were lowest among the WT control, FGL2$^{-/-}$ control, and WT DSS groups, and increased after rFGL2 administration. CYP7A1, the rate-limiting enzyme in BA synthesis in the liver, was detected by IHC and Western blotting. The results showed that CYP7A1 levels in the WT DSS and FGL2$^{-/-}$ DSS groups were higher than those in the WT control and FGL2$^{-/-}$ control groups, respectively. FGL2 knockout further upregulated CYP7A1 levels, whereas rFGL2 treatment downregulated CYP7A1 levels (Fig. 7E–H). These data indicated that FGL2 regulated BA homeostasis in DSS-treated mice.

4. Discussion

Intestinal immune system abnormalities and inflammatory reactions promote the occurrence and development of IBD [5]. FGL2, an immune modulator, plays a great role in inflammatory diseases [24–27]. Our previous studies showed that FGL2 expression was increased in patients with active IBD and a mouse model of colitis [28,29,35]. The increased expression of FGL2 in IBD is probably the result of an important feedback mechanism that cannot control inflammation by itself [36]. Further studies of the role of FGL2 in IBD may provide valuable insight into the etiopathogenesis of IBD and clues for finding new therapeutic strategies. In this study, we showed that FGL2 upregulated the ERK signaling pathway to inhibit LPS-induced inflammation, M1 polarization, autophagy, and apoptosis *in vitro*. The *in vivo* study also demonstrated the effect of FGL2 on experimental UC. FGL2 restrained gut barrier impairment and improved gut microbiota structure and BA metabolism.

The gastrointestinal tract is the largest immune system reservoir in the body, and intestinal macrophages play a role in immune homeostasis as well as inflammation regulation by activating M1 or M2 phenotypes [12,37]. FGL2 was first found in T-regulatory (Treg) cells [38] but is also secreted by macrophages, epithelial cells, dendritic cells, and other cells [39,40]. Our experimental results also showed FGL2 in macrophages. Zhu et al. [36] demonstrated that the elevated FGL2 in colitis was mainly derived from macrophages. All BMDMs were stimulated with LPS to simulate the IBD environment *in vitro*. LPS promoted M1 polarization, inflammation, autophagy, and apoptosis. Our results showed that FGL2 knockout aggravated M1 polarization, inflammation, autophagy, and apoptosis induced by LPS in BMDMs, suggesting that FGL2 can play a great role in regulating M1 polarization and BMDM survival. We used rFGL2 and FGL2 knockout to regulate the expression of FGL2 in BMDMs to investigate the protective effect of FGL2 in LPS-stimulated BMDMs. Our data showed that rFGL2 treatment could reverse the effects of FGL2 knockout and increase the survival of BMDMs. Consistent with our results, studies have also shown that FGL2 inhibited M1 polarization and showed protective effects in mesenchymal stem cells [41] and Kupffer cells [25]. Next, we explored the working mechanism of FGL2 in LPS-stimulated BMDMs. MAPK signaling molecules participate in the signal transmission of various life activities in eukaryotic cells [42], and ERK1/2 is the most widely studied in the classic MAPK pathway. Several studies indicated that FGL2 regulated the MAPK/ERK signaling pathway [43], and ERK was involved in regulating macrophage polarization [44,45] and autophagy [46]. Our study showed that the p-ERK/ERK levels in the FGL2$^{-/-}$ + LPS group were lowest among the control, FGL2$^{-/-}$, and LPS groups and rFGL2 treatment reversed p-ERK/ERK levels. In short, FGL2 inhibited LPS-induced M1 polarization, inflammation, autophagy, and apoptosis *in vitro* through the ERK signaling pathway.

Injury to the intestinal epithelium and the accumulation of inflammatory cells are the main pathological manifestations of IBD [47,48]. In the animal experiments, all mice treated with DSS showed damaged intestinal tissue and significantly increased inflammatory factors. IBD was successfully induced, and we observed that FGL2-deficient mice had more severe colitis from DSS treatment. M1 macrophages are known to secrete cytokines, such as IL-6, IL1β, TNF-α, and iNOS, to induce inflammation [37]. In the DSS model, the level of inflammatory factors was higher in FGL2$^{-/-}$ group mice, and the M1 phenotype in colon tissue increased. However, rFGL2 treatment prevented these changes, indicating that FGL2 can regulate the polarization of macrophages and inhibit inflammation. Also, rFGL2 treatment inhibited inflammation, autophagy, and apoptosis induced by DSS in FGL2$^{-/-}$ mice, and this result further verifies the *in vitro* experimental results. Our results are consistent with previous reports that autophagy activation promotes IBD progression [49,50]. Intestinal macrophage autophagy is abnormally increased when inflammation occurs, leading to the aggravation of IBD [51]. Interestingly, the autophagy level in the FGL2$^{-/-}$ control group was higher than that of the WT control group. We speculate that intestinal macrophages in the FGL2$^{-/-}$ mice may be more prone to M1 phenotype differentiation when they are exposed to an antigen but can still maintain intestinal homeostasis. Tight-junction proteins, including ZO-1 and occludin, are necessary for maintaining the intestinal barrier [52]. When inflammation or oxidative stress reactions increase, ZO-1 and occludin are downregulated, resulting in increased intestinal permeability and impaired intestinal barrier function, which has been proven to be related to IBD [53,54]. However, M1 macrophages cause the breakdown of tight junction proteins, which increases intestinal permeability and leads to excessive inflammation [55]. In our study, FGL2 knockout further downregulated the expression of ZO-1 and occludin in DSS-treated mice, and rFGL2 treatment prevented the breakdown of the intestinal barrier. These results indicated that FGL2 protected the intestinal mechanical barrier and alleviated colitis in DSS-treated mice.

Intestinal flora participate in intestinal metabolism, nutrition, barrier function, and immunity and maintain body homeostasis [56]. 16S rRNA sequencing showed that the bacterial composition of the 2 control groups was not significantly different. After modeling, there were significant differences in bacterial compositions, with reduced beneficial bacteria (*Firmicutes* and *Bacteroidetes*) and increased harmful bacteria (*Proteobacteria*), especially in the FGL2$^{-/-}$ DSS group. These results are consistent with the changes in intestinal microbiota structure observed in IBD patients [16,18,57]. Our study showed that the relative abundance of *Escherichia/-Shigella* in the model mice was upregulated and positively associated with the severity of DSS-related symptoms and actively responded to FGL2 deficiency. *Escherichia/Shigella* is positively correlated with most of the pro-inflammatory parameters in mice and aggravates intestinal leakage by producing alcohol and penetrating the intestinal epithelium, so more toxins and alcohol enter the blood and lymphatic circulations [56,58]. Here, it is preliminarily believed that FGL2 had a certain positive regulatory effect on intestinal bacteria, resulting in the remission of inflammatory reactions. However, the specific mechanism still needs further research.

In this study, the livers of mice in the DSS group showed obvious histological changes, which were also reported by Duan et al. [59] and Zhu et al. [60]. Duboc et al. [17] suggested that gut microbiota imbalance alters BA composition in the gut lumen, which may participate in the chronic inflammation of IBD, and the intestinal secondary BAs of IBD patients decreased, which was more obvious in patients with active IBD. Sinha et al. [61] demonstrated that secondary BA deficiency promoted the development of intestinal inflammation and regulated intestinal ecology. The liver FXR signaling pathway controls the expression of CYP7A1 through negative feedback regulation. The activation of intestinal FXR will promote the secretion of FGF15 in the distal ileum, which inhibits the expression of CYP7A1 [62]. Our results were consistent with these studies. Further, we found that FGL2 deficiency aggravated changes in the above indicators and increased TBA in the serum after DSS modeling. rFGL2 treatment improved BA metabolism. A study found that after healthy volunteers took an FXR agonist (OCA), the abundance of several gram-positive strains increased in the intestine, and endogenous BA synthesis decreased, indicating that FXR activation would change the intestinal microbiota in response to changes in endogenous BA concentrations [63]. Some evidence suggests that ileal FXR activation leads to the stronger inhibition of CYP7A1-mediated BA synthesis than the ctivation of FXR in the liver [62,64]. However, altered gut microbiota structure affects Bile Salt Hydrolase enzymatic activity and inhibits intestinal FXR [65].

Although we found that FGL2 improved gut microbiota structure and BA metabolism in DSS-treated mice, the relationship between intestinal microflora and BA is still unclear. Thus, the causal and mechanism of FGL2, gut microbiota, and bile acid will be our next research direction.

5. Conclusions

Our study provides a new perspective for the protective mechanism of FGL2 on IBD. In the future, FGL2 may become a biomarker or therapeutic target for IBD treatment.

Data availability statement

we are uploading the data associated with our study in NCBI. After the article is published, the data number will be supplemented and updated in online version.

Ethics declarations

This study was reviewed and approved by the Experimental Animal Management Committee of Wenzhou Medical University, with the approval number: WYDW20170074.

CRediT authorship contribution statement

Yuan Zhao: Writing – original draft, Visualization, Validation, Investigation, Formal analysis, Data curation. **Zheng Xiang:** Resources, Investigation, Data curation. **Haoran Pan:** Resources, Investigation. **Xielin Huang:** Formal analysis. **Weizhen Chen:** Resources. **Zhiming Huang:** Writing – review & editing, Supervision, Project administration, Methodology, Funding acquisition, Conceptualization.

Declaration of competing interest

The authors declare the following financial interests/personal relationships which may be considered as potential competing interests:Zhiming Huang reports article publishing charges, equipment, drugs, or supplies, and writing assistance were provided by First Affiliated Hospital of Wenzhou Medical University. If there are other authors, they declare that they have no known competing financial interests or personal relationships that could have appeared to influence the work reported in this paper.

Acknowledgements

Appendix A. Supplementary data

Supplementary data to this article can be found online at https://doi.org/10.1016/j.heliyon.2024.e34349.

References

[1] N. Seyed Tabib, et al., Big data in IBD: big progress for clinical practice, Gut 69 (8) (2020) 1520–1532.
[2] G. Roda, et al., Crohn's disease, Nat. Rev. Dis. Prim. 6 (1) (2020) 22.
[3] L. Prideaux, et al., Inflammatory bowel disease in Asia: a systematic review, J. Gastroenterol. Hepatol. 27 (8) (2012) 1266–1280.

[4] N. Molodecky, et al., Increasing incidence and prevalence of the inflammatory bowel diseases with time, based on systematic review, Gastroenterology 142 (1) (2012) 46–54, e42; quiz e30.

[5] P. Nash, et al., Points to consider for the treatment of immune-mediated inflammatory diseases with Janus kinase inhibitors: a consensus statement, Ann. Rheum. Dis. 80 (1) (2021) 71–87.

[6] D. Owczarek, et al., Diet and nutritional factors in inflammatory bowel diseases, World J. Gastroenterol. 22 (3) (2016) 895–905.

[7] J. Lloyd-Price, et al., Multi-omics of the gut microbial ecosystem in inflammatory bowel diseases, Nature 569 (7758) (2019) 655–662.

[8] F. Ryan, et al., Colonic microbiota is associated with inflammation and host epigenomic alterations in inflammatory bowel disease, Nat. Commun. 11 (1) (2020) 1512.

[9] S. Shah, S. Itzkowitz, Colorectal cancer in inflammatory bowel disease: mechanisms and management, Gastroenterology 162 (3) (2022) 715–730.e3.

[10] C. Shailja, S.H.I. Shah, Colorectal cancer in inflammatory bowel disease: mechanisms and management, Gastroenterology 162 (3) (2022) 715–730 e3.

[11] M. Elliott, K. Koster, P. Murphy, Efferocytosis signaling in the regulation of macrophage inflammatory responses, J. Immunol. 198 (4) (2017) 1387–1394.

[12] Y. Zheng, et al., Intestinal macrophage autophagy and its pharmacological application in inflammatory bowel disease, Front. Pharmacol. 12 (2021) 803686.

[13] S. Sánchez-Fidalgo, et al., Abarema cochliacarpos reduces LPS-induced inflammatory response in murine peritoneal macrophages regulating ROS-MAPK signal pathway, J. Ethnopharmacol. 149 (1) (2013) 140–147.

[14] E. Russo, et al., Immunomodulating activity and therapeutic effects of short chain fatty acids and tryptophan post-biotics in inflammatory bowel disease, Front. Immunol. 10 (2019) 2754.

[15] T. Zelante, et al., Tryptophan catabolites from microbiota engage aryl hydrocarbon receptor and balance mucosal reactivity via interleukin-22, Immunity 39 (2) (2013) 372–385.

[16] M. Poletti, et al., Organoid-based models to study the role of host-microbiota interactions in IBD, Journal of Crohn's & colitis 15 (7) (2021) 1222–1235.

[17] H. Duboc, et al., Connecting dysbiosis, bile-acid dysmetabolism and gut inflammation in inflammatory bowel diseases, Gut 62 (4) (2013) 531–539.

[18] K. Wallace, et al., Immunopathology of inflammatory bowel disease, World J. Gastroenterol. 20 (1) (2014) 6–21.

[19] Y. Okada, et al., Propionibacterium freudenreichii component 1.4-dihydroxy-2-naphthoic acid (DHNA) attenuates dextran sodium sulphate induced colitis by modulation of bacterial flora and lymphocyte homing, Gut 55 (5) (2006) 681–688.

[20] N. Osman, et al., Bifidobacterium infantis strains with and without a combination of oligofructose and inulin (OFI) attenuate inflammation in DSS-induced colitis in rats, BMC Gastroenterol. 6 (2006) 31.

[21] S. Ukena, et al., Probiotic Escherichia coli Nissle 1917 inhibits leaky gut by enhancing mucosal integrity, PLoS One 2 (12) (2007) e1308.

[22] J. Zhou, et al., Effect of fecal microbiota transplantation on experimental colitis in mice, Exp. Ther. Med. 17 (4) (2019) 2581–2586.

[23] J. Hu, et al., The duality of Fgl2 - secreted immune checkpoint regulator versus membrane-associated procoagulant: therapeutic potential and implications, Int. Rev. Immunol. 35 (4) (2016) 325–339.

[24] Y. Zhou, et al., Fibrinogen-like protein 2 controls sepsis catabasis by interacting with resolvin Dp5, Sci. Adv. 5 (11) (2019) eaax0629.

[25] G. Pan, et al., Soluble fibrinogen-like protein 2 ameliorates acute rejection of liver transplantation in rat via inducing Kupffer cells M2 polarization, Cancer Med. 7 (7) (2018) 3168–3177.

[26] D. Clark, et al., The fgl2 prothrombinase/fibroleukin gene is required for lipopolysaccharide-triggered abortions and for normal mouse reproduction, Mol. Hum. Reprod. 10 (2) (2004) 99–108.

[27] I. McGilvray, et al., Murine hepatitis virus strain 3 induces the macrophage prothrombinase fgl-2 through p38 mitogen-activated protein kinase activation, J. Biol. Chem. 273 (48) (1998) 32222–32229.

[28] X. Dong, et al., Fibrinogen-like protein 2 prothrombinase may contribute to the progression of inflammatory bowel disease by mediating immune coagulation, Int. J. Clin. Exp. Pathol. 11 (3) (2018) 1629–1636.

[29] X. Dong, et al., Intestinal and peripheral fibrinogen-like protein 2 expression in inflammatory bowel disease, Dig. Dis. Sci. 59 (4) (2014) 769–777.

[30] B. Chassaing, et al., Dextran sulfate sodium (DSS)-induced colitis in mice, Curr. Protoc. Im. 104 (2014) 15.25.1–15.25.14.

[31] A. Bartczak, et al., Overexpression of fibrinogen-like protein 2 promotes tolerance in a fully mismatched murine model of heart transplantation, Am. J. Transplant. : official journal of the American Society of Transplantation and the American Society of Transplant Surgeons 16 (6) (2016) 1739–1750.

[32] X. Chen, et al., Lactulose mediates suppression of dextran sodium sulfate-induced colon inflammation by increasing hydrogen production, Dig. Dis. Sci. 58 (6) (2013) 1560–1568.

[33] W. Ying, et al., Investigation of macrophage polarization using bone marrow derived macrophages, J. Vis. Exp. (76) (2013).

[34] S.F. Luca Santucci, Natalia Rubinstein, Andrea Mencarelli, Barbara Palazzetti, Barbara Federici, Gabriel A. Rabinovich, Antonio Morelli, Galectin-1 suppresses experimental colitis in mice, Gastroenterology 124 (5) (2003) 1381–1394.

[35] H. Lin, et al., Elevated fibrinogen-like protein 2 in TNBS-induced colitis mice: association with Th17 and regulatory T cells, Mol. Med. Rep. 16 (3) (2017) 3445–3454.

[36] Y. Zhu, et al., Control of intestinal inflammation, colitis-associated tumorigenesis, and macrophage polarization by fibrinogen-like protein 2, Front. Immunol. 9 (2018) 87.

[37] Q. Hu, et al., Extracellular vesicle activities regulating macrophage- and tissue-mediated injury and repair responses, Acta Pharm. Sin. B 11 (6) (2021) 1493–1512.

[38] S. Marazzi, et al., Characterization of human fibroleukin, a fibrinogen-like protein secreted by T lymphocytes, J. Immunol. 161 (1) (1998) 138–147.

[39] C. Yang, et al., Expression of B and T lymphocyte attenuator (BTLA) in macrophages contributes to the fulminant hepatitis caused by murine hepatitis virus strain-3, Gut 62 (8) (2013) 1204–1213.

[40] K. Su, et al., Fibrinogen-like protein 2/fibroleukin prothrombinase contributes to tumor hypercoagulability via IL-2 and IFN-gamma, World J. Gastroenterol. 14 (39) (2008) 5980–5989.

[41] C. Gao, et al., Mesenchymal stem cells transfected with sFgl2 inhibit the acute rejection of heart transplantation in mice by regulating macrophage activation, Stem Cell Res. Ther. 11 (1) (2020) 241.

[42] L. Osaki, P. Gama, MAPKs and signal transduction in the control of gastrointestinal epithelial cell proliferation and differentiation, Int. J. Mol. Sci. 14 (5) (2013) 10143–10161.

[43] Y. Liu, et al., Downregulation of FGL2/prothrombinase delays HCCLM6 xenograft tumour growth and decreases tumour angiogenesis, Liver Int. : official journal of the International Association for the Study of the Liver 32 (10) (2012) 1585–1595.

[44] C. Liu, B. Su, J. Chen, Gardnerella vaginalisTilapia piscidin 4 (TP4) reprograms M1 macrophages to M2 phenotypes in cell models of -induced vaginosis, Front. Immunol. 12 (2021) 773013.

[45] S. Ruan, et al., Nicotine alleviates MPTP-induced nigrostriatal damage through modulation of JNK and ERK signaling pathways in the mice model of Parkinson's disease, Front. Pharmacol. 14 (2023) 1088957.

[46] C. Kinsey, et al., Protective autophagy elicited by RAF→MEK→ERK inhibition suggests a treatment strategy for RAS-driven cancers, Nat. Med. 25 (4) (2019) 620–627.

[47] S. Lee, J. Kwon, M. Cho, Immunological pathogenesis of inflammatory bowel disease, Intestinal research 16 (1) (2018) 26–42.

[48] M. Leppkes, M. Neurath, Cytokines in inflammatory bowel diseases - update 2020, Pharmacol. Res. 158 (2020) 104835.

[49] Y.S. Zhang, et al., Natural dietary compound naringin prevents azoxymethane/dextran sodium sulfate-induced chronic colorectal inflammation and carcinogenesis in mice, Cancer Biol. Ther. 19 (8) (2018) 735–744.

[50] S. Wang, et al., Intestinal autophagy links psychosocial stress with gut microbiota to promote inflammatory bowel disease, Cell Death Dis. 10 (6) (2019) 391.

[51] H. Chu, et al., Gene-microbiota interactions contribute to the pathogenesis of inflammatory bowel disease, Science (New York, N.Y.) 352 (6289) (2016) 1116–1120.

[52] M. Odenwald, J. Turner, *The intestinal epithelial barrier: a therapeutic target?* Nature reviews, Gastroenterol. Hepatol. 14 (1) (2017) 9–21.

[53] S. Mehandru, J. Colombel, The intestinal barrier, an arbitrator turned provocateur in IBD, Nat. Rev. Gastroenterol. Hepatol. 18 (2) (2021) 83–84.

[54] W. Turpin, et al., Increased intestinal permeability is associated with later development of crohn's disease, Gastroenterology 159 (6) (2020) 2092–2100.e5.

[55] S. Ma, et al., The role of tissue-resident macrophages in the development and treatment of inflammatory bowel disease, Front. Cell Dev. Biol. 10 (2022) 896591.

[56] F. Shen, et al., Gut microbiota dysbiosis in patients with non-alcoholic fatty liver disease, Hepatobiliary Pancreat. Dis. Int. : HBPD INT 16 (4) (2017) 375–381.

[57] D. Frank, et al., Molecular-phylogenetic characterization of microbial community imbalances in human inflammatory bowel diseases, Proc. Natl. Acad. Sci. U.S. A. 104 (34) (2007) 13780–13785.

[58] C. Zhao, et al., Commensal cow Roseburia reduces gut-dysbiosis-induced mastitis through inhibiting bacterial translocation by producing butyrate in mice, Cell Rep. 41 (8) (2022) 111681.

[59] S. Duan, et al., Effect of vitexin on alleviating liver inflammation in a dextran sulfate sodium (DSS)-induced colitis model, Biomedicine & pharmacotherapy = Biomedecine & pharmacotherapie 121 (2020) 109683.

[60] L. Zhu, et al., Multi-Omics analysis of the gut-liver Axis reveals the mechanism of liver injury in colitis mice, Front. Immunol. 12 (2021) 773070.

[61] S. Sinha, et al., Dysbiosis-induced secondary bile acid deficiency promotes intestinal inflammation, Cell Host Microbe 27 (4) (2020) 659–670.e5.

[62] I. Kim, et al., Differential regulation of bile acid homeostasis by the farnesoid X receptor in liver and intestine, J. Lipid Res. 48 (12) (2007) 2664–2672.

[63] E. Friedman, et al., FXR-dependent modulation of the human small intestinal microbiome by the bile acid derivative obeticholic acid, Gastroenterology 155 (6) (2018) 1741–1752.e5.

[64] B. Kong, et al., Mechanism of tissue-specific farnesoid X receptor in suppressing the expression of genes in bile-acid synthesis in mice, Hepatology (Baltimore, Md 56 (3) (2012) 1034–1043.

[65] A. Wahlström, et al., Intestinal crosstalk between bile acids and microbiota and its impact on host metabolism, Cell Metabol. 24 (1) (2016) 41–50.